Structural and magnetic properties of (Ga,Mn)N from first principles

Teemu Hynninen,* Hannes Raebiger,† and Juhani von Boehm
COMP/Laboratory of Physics, Helsinki University of Technology, P.O. Box 1100, 02015 HUT, Finland
(Received 7 December 2006; published 26 March 2007)

The structure of Mn clusters in (Ga,Mn)N and the interactions of the magnetic Mn ions and clusters are studied using first-principles calculations. Curie temperatures are calculated using mean-field and Monte Carlo methods. It is found that joining substitutional Mn ions to clusters is energetically favorable and especially the structures of two to four Mn ions formed around a single N ion are most stable. These clusters are always found to have a ferromagnetic ground state, and ferromagnetic intercluster interactions are also present even at relatively long distances. For randomly distributed Mn impurities, high Curie temperatures are obtained at high Mn concentrations (above room temperature for $x \gtrsim 0.14$).

DOI: 10.1103/PhysRevB.75.125208 PACS number(s): 75.50.Pp, 75.40.Mg, 85.75.−d

I. INTRODUCTION

Diluted magnetic semiconductors (DMS's) have attracted much interest since ferromagnetism was discovered in (In,Mn)As.[1] DMS materials with high Curie temperatures (T_C's) could be valuable in spintronics technology,[2] but the realization of room-temperature ferromagnetism in DMS's has been difficult. Using a Zener model, Dietl *et al.*[3] predicted the T_C of (Ga,Mn)N to be among the highest obtainable in DMS's. As a result, much research has been devoted to studying (Ga,Mn)N, but still many properties of this material are poorly understood. The experimental results for the T_C in (Ga,Mn)N vary from 0 to 900 K,[4–9] and the critical temperature seems to depend not only on the Mn concentration x in $Ga_{1-x}Mn_xN$ but also on the growth conditions and the resulting microstructure in a complex way. It has been suggested that the observed high values of T_C are caused by the formation of ferromagnetic Mn precipitates or Mn clusters with large magnetic moments.[10–12] Indeed, at any adequately high x, a considerable number of small Mn clusters are present in the system even if the substitutional Mn ions are distributed completely randomly.[13] First-principles calculations have also indicated that it is energetically favorable for substitutional Mn ions to cluster around the N ions,[10,14] and therefore, in a real system the Mn ions should show a strong tendency to form more clusters.[13] However, the formation of Mn clusters is often also reported to decrease the theoretically calculated T_C's.[13,15–19] Thus, it is of interest to systematically investigate the structural properties of Mn clusters in (Ga,Mn)N as well as the magnetic interactions between different clusters. We focus on substitutional Mn ions, as Mn is experimentally found to occupy Ga sites,[9] and denote the substitutional Mn ions simply by Mn. In this paper, we distinguish two types of clusters (denoted by Mn_n, $n=1,2,\ldots$): When discussing structural properties, we consider in general groups of Mn ions where the ions are linked to each other by Mn–N–Mn bonds. We call these groups Mn complexes. In our Monte Carlo approach, we limit ourselves to groups of Mn ions where all the ions share a common nearest neighbor N ($n \leqslant 4$). These are called clusters in the text. In this paper, we do not consider Mn complexes which involve, e.g., vacancies or interstitials.

In order to predict the Curie temperature of (Ga,Mn)N and how the microstructure influences it, we study the structural and magnetic properties of clusters of up to four Mn ions using first-principles methods. Based on the results, we identify the stable Mn configurations and study the energetics involved in cluster formation. The magnetic properties of the clusters are examined by comparing the total energies of various spin configurations to determine the strength of exchange interactions both between Mn ions inside the clusters and between the entire clusters (intracluster and intercluster exchanges, respectively). We map the calculated spin-flip energies onto a modified Heisenberg Hamiltonian which is then used in Monte Carlo simulation to extract the T_C's at various Mn concentrations and cluster configurations. As a comparison, we also apply the simple mean-field approximation. Some of the results in this paper have appeared in short papers (Refs. 12 and 13).

II. METHODS

A. Electronic structure calculations

We perform spin-polarized total-energy supercell calculations for (Ga,Mn)N in the wurtzite structure using the density-functional theory (DFT) and applying the all-electron projector augmented-wave (PAW) method as implemented in the VASP plane-wave code.[20] We treat exchange correlation in the generalized gradient approximation (GGA-PW91) as well as in the on-site corrected local-spin-density approximation[21] (LSDA+U). We compare the two methods since in the ordinary LSDA or GGA, self-interaction effects are present for the localized Mn d states and may therefore strongly affect the results.[22,23] The on-site correction is only applied to Mn d states for which the parameter U is chosen to be 3 eV (Refs. 22 and 23) except when explicitly stated otherwise.

To verify numerical convergence, we have carried out test calculations for the plane-wave cutoff energy and the Brillouin-zone sampling. We apply the linear tetrahedron method with Bloechl corrections for calculating integrals over the Brillouin zone, and the corresponding k meshes are generated using the Γ-centered Monkhorst-Pack scheme.[24] The required mesh density was studied in a hexagonal $Ga_{35}N_{36}Mn_1$ supercell. For this system, a $4\times4\times4$ mesh was found to be sufficient. When calculating cells of other sizes

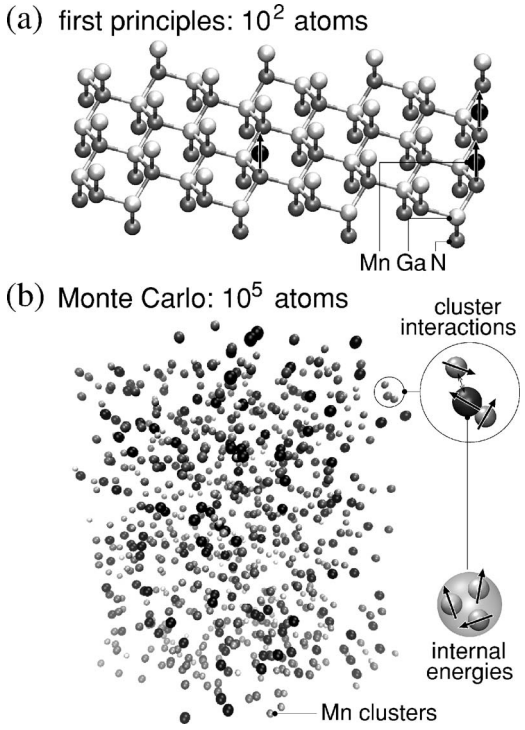

FIG. 1. A schematic illustration of the used scales. (a) Accurate first-principles calculations are restricted to small supercells, (b) while Monte Carlo simulation enables analysis of mesoscopic behavior using large cells (with only Mn clusters visible). In (b), the shades of gray denote cluster sizes (the size grows from one to four Mn as the color changes from white to black).

or shapes, we scale the k mesh accordingly to maintain an approximately constant k-point density in the reciprocal space. For the plane-wave cutoff, we use the energy of 425 eV. These parameters result in an accuracy of a few meV for the total energy of the supercell. Local properties such as projected densities of states (DOSs) are calculated by projecting the wave functions to the corresponding spherical harmonics.[25] The Wigner-Seitz radii used in the projections for Mn and N sites are 1.3 and 0.7 Å, respectively.

B. Curie temperature calculations

The Curie temperature is a thermodynamic phase transition point and therefore only relevant in macroscopic systems. The first-principles results are restricted to systems of roughly 100 atoms [see Fig. 1(a)] and to calculate T_C, we must use either analytic expressions or numerical analysis of mesoscopic systems combined with finite-size scaling. In this paper, we apply both Monte Carlo (MC) analysis and the simple mean-field approximation (MFA). The MC calculations are carried out in supercells which are constructed of $L\times L\times L$ four-atom wurtzite unit cells where $L=24,\ldots,36$ [an example of a MC supercell is shown in Fig. 1(b)].

We use a modified Heisenberg Hamiltonian to describe the system as a collection of Mn clusters; i.e., we separate the intercluster and intracluster interactions in the Hamiltonian [Fig. 1(b)]. Since Mn ions and clusters have large spins, the use of a classical model is justified.[26] The effective spin of the ith cluster with n_i Mn ions is defined as $\mathbf{s}_i=\Sigma_k^{n_i}\mathbf{e}_{ik}/n_i$, where the unit vectors $\mathbf{e}_{ik}$ are the Mn spins. It is assumed that the exchange coefficients for the intercluster coupling depend only on cluster sizes and separations, $J_{ij}=J_{n_in_j}(r_{ij})$. Furthermore, as we shall show, the intracluster interactions are poorly described by the Heisenberg model and therefore we write the internal energies using functions $E_{n_i}(s_i)$ instead. Thus, our effective Hamiltonian is of the form

$$H=-\sum_{(i,j)}J_{n_in_j}(r_{ij})\mathbf{s}_i\cdot\mathbf{s}_j-\sum_i E_{n_i}(s_i). \tag{1}$$

A more detailed description of the model and the fitting of the parameters are given in the Appendix.

The Monte Carlo simulations using the Hamiltonian [Eq. (1)] are carried out using a combined Wolff-Metropolis algorithm, where the cluster spins $\mathbf{s}_i$ are sampled using the Wolff method[27] and the ionic spins $\mathbf{e}_{ik}$ using the Metropolis scheme.[28] Ergodicity is maintained by frequently switching between the two algorithms. The actual T_C^{MC} values are found using the cumulant crossing method[29] in which the Curie point is determined by the temperature where the cumulants $U_L(T)\sim\langle M^4\rangle/\langle M^2\rangle^2$ (M being the magnetization) with different L cross. To account for geometric disorder, we randomly position the required number of Mn clusters in the cell and calculate the geometric average over 20–50 replications.

Simple estimates for the Curie temperature within the MFA are given by[30–32]

$$T_C^{\mathrm{MFA}}=\frac{1}{3k_B}\sum_j J_{0j}\approx\frac{2}{3k_B}\frac{\Delta E}{N}=T_C^{\Delta E}, \tag{2}$$

where $\Delta E/N=(E_{\mathrm{AF}}-E_{\mathrm{FM}})/N$ is the energy difference between ferromagnetic (FM) and antiferromagnetic (AF) spin configurations per magnetic particle and k_B is the Boltzmann constant. The approximation allows us to roughly estimate the Curie points of the periodic systems represented by the supercells used in first-principles calculations by treating Mn clusters as the primary magnetic entities.[12] Thus, in Eq. (2) $N=2$ (the number of Mn clusters in a DFT supercell) and ΔE is the calculated energy needed to flip the spin of one of the clusters.

To be accurate, ΔE in Eq. (2) should be the energy difference between a ferromagnetic and a magnetically disordered (D) system with $E_D=0$, since the energy of the FM state is $E_{\mathrm{FM}}/N=-1/N\times\Sigma_{i\neq j}J_{ij}/2=-\Sigma_j J_{0j}/2$ if the clusters have similar neighborhoods. The energy E_{AF} of the AF state depends on the interactions: for very-long-ranged coupling (as assumed in MFA), $E_{\mathrm{AF}}/N\approx 0$ and $\Delta E/N\approx\Sigma_j J_{0j}/2$, but if the nearest-neighbor interactions dominate, $E_{\mathrm{AF}}/N\approx\Sigma_j J_{0j}/2$ and $\Delta E/N\approx\Sigma_j J_{0j}$ which leads to an error. To distinguish the T_C^{MFA} evaluated using the sum of J's as opposed to ΔE, we denote the latter by $T_C^{\Delta E}$.

III. STRUCTURAL PROPERTIES

A. Configurations of Mn clusters

In order to study the structural properties of Mn complexes, we first geometrically optimize the GaN wurtzite lat-

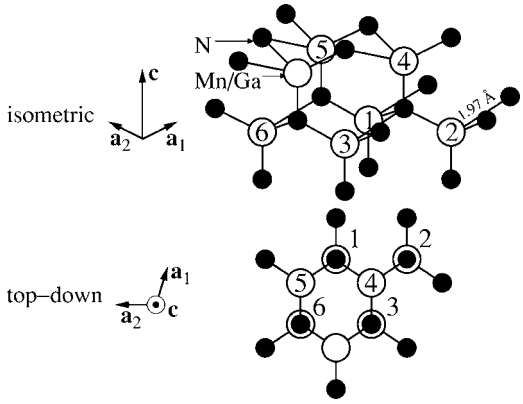

FIG. 2. Wurtzite structure from isometric and top-down perspectives.

tice (see Fig. 2) by minimizing the total energy using GGA. As a result, we find the lattice constants $a=3.217$ Å and $c:a=1.631$ in reasonable agreement with experimental values of 3.189 Å and 1.626, respectively.[33] The corresponding calculated nearest-neighbor Ga-Ga and Ga-N bond lengths are 3.22 and 1.97 Å, respectively. We adopt these optimized values for the calculations presented in this paper. We also introduce the convention of calling the crystallographic plane (0001) the a plane (since it is spanned by the symmetric vectors $\mathbf{a}_1$ and $\mathbf{a}_2$ with length a, see Fig. 2) and the perpendicular direction the c axis. The actual structural optimization of different complexes up to four Mn ions is carried out in a 72 atom supercell and the resulting structures for the energetically most favorable complexes are shown in Fig. 3. All these structures are found to have a ferromagnetic ground state. We discuss the magnetic properties in more detail in Sec. IV.

A dimer (Mn_2) consists of two Mn ions either in the same a plane or tilted in the c direction [see Fig. 3(a)]. We find the a-plane dimer to be the energetically favorable configuration although the energy difference between the two dimers is only 27 meV. For trimers (Mn_3), there are several possible configurations, but we only consider the most compact cases where the Mn ions either surround one N ion in a star-shaped pattern or form a ring with three N ions [referring to the labeling in Fig. 2, the sites (1,2,3) or (1,2,4) form a star and sites (1,3,6) or (1,4,5) form a ring]. As with the dimers, trimers may lie completely in the a plane or they can also be tilted in the c direction. We find the star-shaped (N-centered) configuration in the a plane to have the lowest total energy of these trimers although the energy of the tilted star-shaped trimer is only 39 meV higher [Fig. 3(b)]. On the other hand, energies of the a plane and tilted ring trimers are 220 and 181 meV higher, respectively. For tetramers (Mn_4), we consider tetrahedron and planar shapes [sites (1,2,3,4) and (1,2,3,6), respectively]. In this case, we find the total energy of the tetrahedron [Fig. 3(c)] to be as much as 337 meV lower than the energy of the planar tetramer, showing again that a N-centered cluster is the preferred structure.

Bond lengths obtained by structural optimization are also shown in Fig. 3 for the most stable complexes. The simplest Mn structure is the monomer (Mn_1), i.e., a single substitutional Mn ion with no other Mn neighbors (not shown). Optimizing the structure using the GGA functional we find the elongated Mn–N bond lengths of 1.98 and 2.02 Å for the three symmetric bonds and the one asymmetric bond (along the c axis), respectively. Similar to Mn_1, we find that the optimized Mn–N bond lengths around the clusters, $1.97,\ldots,2.01$ Å (see Fig. 3), are longer than the bulk Ga–N bonds of 1.97 Å. On the other hand, we find that whenever a N ion is located between two Mn ions, i.e., when the bond is inside a Mn complex, the Mn–N bonds, $1.91,\ldots,1.94$ Å (Fig. 3), are somewhat shorter than the bulk Ga–N bonds. Similarly, the Mn-Mn distances of $3.10,\ldots,3.17$ Å (Fig. 3) are shorter compared to the corresponding bulk Ga-Ga separations of 3.22 Å.

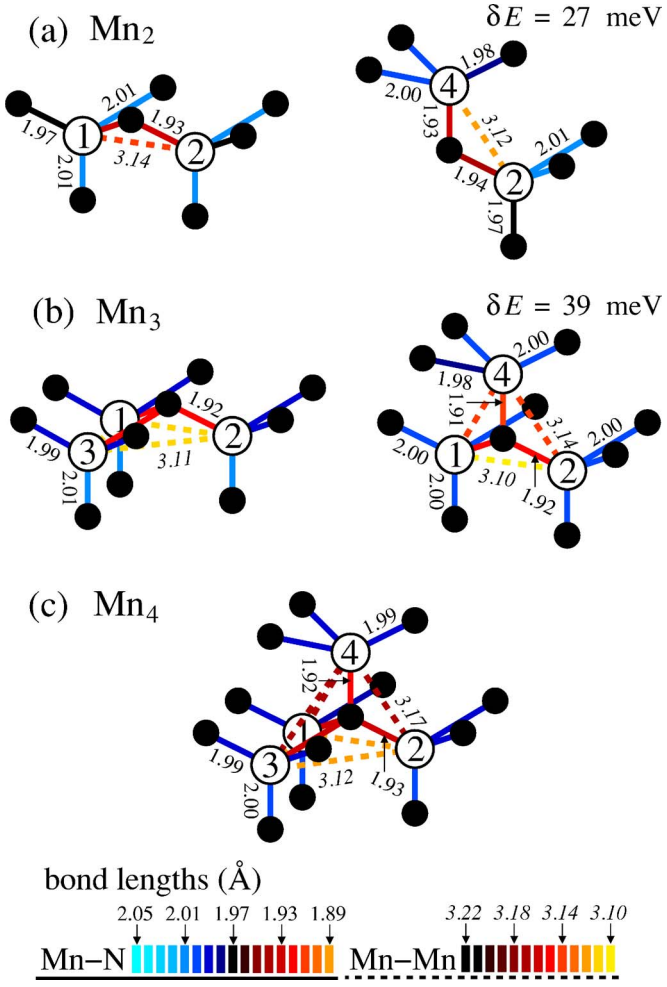

FIG. 3. (Color online) (a)–(c) Structurally optimized geometries for the energetically most stable complexes (clusters) of two to four Mn ions. The Mn sites are numbered according to Fig. 2. Bond lengths are shown both as numbers (in Å) and using different colors, black corresponds to bonds in GaN. In (a) and (b), the first structure is lowest in energy and the δE's give the energies with respect to them.

The shortening of the intracluster Mn–N bonds and the elongation of the Mn–N bonds surrounding complexes may be qualitatively understood by comparing to the fully relaxed MnN wurtzite crystal lattice where the Mn substitution is complete. We obtain for the theoretical antiferromagnetic wurtzite MnN the Mn–Mn bond length of 3.06 and the

Mn–N bond length of 1.87 Å. In Ref. 34, the lattice parameters for the wurtzite MnN, calculated using similar methods as in this paper, are reported to be $a=2.97,\ldots,3.03$ Å and $c=4.95,\ldots,5.22$ Å depending on the magnetic phase. These correspond to Mn–Mn bonds of $3.0,\ldots,3.1$ Å and Mn–N bonds of around 1.9 Å, in agreement with our values. These calculated bond lengths suggest that in (Ga,Mn)N, the nearest intracluster Mn-Mn distances have a tendency to get shorter than the Ga-Ga bulk distances, and this is exactly what we find ($3.10,\ldots,3.17$ Å <3.22 Å). The reason why the intracluster Mn-Mn distances are slightly longer than those of the ideal wurtzite MnN crystal lattice may be related to the relatively rigid bulk GaN lattice around the Mn clusters preventing full relaxation. We also observe that the positions of Mn ions deviate from those of the ideal GaN lattice less in the ring-shaped trimers (not shown) compared to the star-shaped ones: in the rings, we get the Mn–Mn and intracluster Mn–N bonds of $3.14,\ldots,3.20$ Å and $1.94,\ldots,1.97$ Å, respectively. Apparently, the coupling to the surrounding bulk GaN is stronger in the rings preventing the relaxation of the Mn ions.

As for the experiments, in Ref. 35 the Mn–N bond length is found to be 2.07 Å, 0.12 Å longer than the Ga-N distance. Another experimental study gives the values of $1.98,\ldots,2.01$ Å.[36] These values should correspond to our Mn–N bonds surrounding the clusters because they form the clear majority of the Mn–N bonds. Indeed, our calculated values of $1.97,\ldots,2.01$ Å agree quite closely with these experiments, especially those of Ref. 36. In Ref. 37, the calculated first-principles intracluster Mn–N bonds of $1.98,\ldots,1.99$ Å are obtained for a dimer in bulk. These are longer than the used experimental Ga-N length of 1.95 Å. We find the Mn-N length of 1.93 Å [Fig. 3(a)] which is shorter than our Ga-N length. The difference may be due to the different lattice constants and lower plane-wave cutoff energies used in Ref. 37.

B. Formation of Mn clusters

To estimate how favorable it is for the Mn ions to form clusters, we calculate the binding energies E_b of Mn ions in the energetically most stable complexes. This is done using 72 atom $Ga_{36-n}N_{36}Mn_n$ supercells, $n=2$, 3, or 4, where we set a Mn_{n-1} complex and a Mn monomer as far apart as possible (around 7 Å) and compare the total energy to that of one Mn_n complex: $E_b=E(Mn_{n-1}+Mn)-E(Mn_n)$. We calculate E_b also for $n=5,6$, but in these cases we apply a 108 atom supercell without structural optimization. The calculated E_b are shown in Fig. 4 (filled squares and diamonds for optimized and unoptimized geometries, respectively). In order to see the effect of the optimization and the cell size, the case $n=4$ is calculated in both supercells and both with and without optimization in the smaller cell. The obtained E_b are 622, 653, and 720 meV for the optimized and unoptimized 72 atom systems and the 108 atom system, respectively. The calculated E_b is higher in the larger cell since the single Mn is separated farther from the complex. However, optimizing the structure changes the energy by only 5% so the lack of structural optimization is a justified approximation. This was to be expected since the positions of the Mn ions do not change very much in the optimization (see Fig. 3).

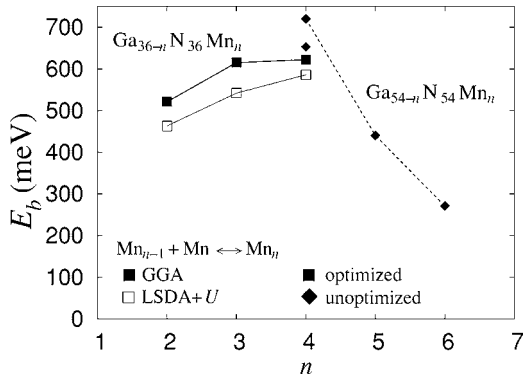

FIG. 4. Binding energies E_b of Mn ions in Mn_n complexes. The cases $n\leqslant 4$ (squares) are calculated in a 72 atom $Ga_{36-n}N_{36}Mn_n$ supercell with structural optimization, while for $n\geqslant 4$ a 108 atom $Ga_{54-n}N_{54}Mn_n$ supercell is used without optimization (diamonds). The unconnected diamond at $n=4$ is calculated in a 72 atom supercell without structural optimization. GGA values for $n=2$, 3, and 4 (72 atom supercell) are from Ref. 13.

We always find clustering to be energetically favorable, $E_b>0$, but there is a maximum at $n=4$ corresponding to tetramer formation. The drop in E_b for larger n may be understood on the basis of the configurational energies of smaller complexes: it is always most favorable to join the Mn ions closely around one central N ion. However, after completing the tetrahedral tetramer, this is no longer possible and the next Mn ion must be set to a more loosely bound position. It should be noted that the case $n=6$ in Fig. 4 is calculated for a geometry where two Mn ions are set on different sides of a Mn_4 tetrahedron. Should the Mn ions be set next to each other, the binding energy should be higher. Still, the high-symmetry tetrahedron-shaped tetramer is an especially stable configuration. We have calculated the binding energies also using LSDA+U up to tetramer formation and the results are slightly lower but still very close to those given by GGA (Fig. 4, open squares).

Even when Ga ions are wholly randomly substituted by Mn ions (at a given concentration x), a considerable percentage of the Mn ions will form dimers and also some larger complexes as well.[12,18] As the formation of Mn_n complexes is energetically favorable, we expect that an even higher portion of the Mn ions will form complexes in a real system. Such a tendency is seen in lattice gas MC simulations, which predict that at a 1000 K thermal equilibrium, there will be few monomers (about 10% of clusters) and a considerable number of dimers, trimers, and tetramers (15%–40% each, when only considering the N-centered clusters).[13] Since the highest E_b is found for trimers and tetramers, it is possible that the clustering favors these sizes at least if the Mn concentration x is not very large (Fig. 4). This agrees with Ref. 14, where the heat of reaction $E_h=E(Mn_{n-1}+Mn_{n+1})-E(2Mn_n)$ is found to change sign at $n\approx 3$, suggesting that trimers are the most stable complexes. Since N-centered Mn clusters are the most important type of complexes, we focus on these clusters in the following sections.

IV. MAGNETIC PROPERTIES

A. Intracluster spin-flip energies

In order to study the magnetic properties of single Mn_n clusters, we calculate internal spin-flip energies by comparing the total energies of various collinear spin configurations. We set up a 72 atom supercell with one Mn_2, Mn_3, or Mn_4 cluster inside and calculate the energies of nonequivalent spin configurations. Due to rotational and spin symmetries, there are only two such configurations for the *a*-plane dimer and trimer: the ferromagnetic one and a configuration where one spin is flipped. On the other hand, because of the asymmetry in the *c* direction, there are three symmetric spins and one asymmetric spin in a tetrahedral tetramer. Therefore, there are two ferrimagnetic configurations where one spin has been flipped and one antiferromagnetic state where two spins have been flipped.

The total magnetic moment of a supercell in a ferromagnetic state is always found to be n (the number of Mn ions) times $4\mu_B$ regardless of the cluster size and used exchange-correlation functional. (The integer magnetic moment is a consequence of the minority-spin channel having no partially filled electronic bands which dictates that there cannot be a noninteger occupation in the majority channel either.) On the other hand, the distribution of magnetization density does depend on the value of U. The largest contribution to the magnetic moment comes from Mn d states whose localization is enhanced by the U correction. Thus, while the local GGA magnetic moment at a Mn ion (in an atomic sphere) is on average $3.5\mu_B$, the local LSDA+U moment increases up to $4.4\mu_B$ for $U=7$ eV. This change is compensated by inducing small antiparallel magnetic moments to the N p states at the neighboring sites, in qualitative agreement with Refs. 23 and 38.

We always find the ground state to be ferromagnetic, but as n increases from 2 to 4, the calculated spin-flip energies are found to decrease linearly with n from 307 (spin-flip energy for a Mn spin inside a dimer) to 226 (trimer) and 123 or 131 meV (symmetric and asymmetric spins in a tetramer, respectively). Furthermore, flipping two spins in a tetramer costs 401 meV in showing that the second spin flip requires an energy of 278 or 270 meV, i.e., more than twice the energy needed for the first flip. Thus, in agreement with Ref. 14, this demonstrates that a simple Heisenberg model fails to describe the intracluster spin-flip energies since with ferromagnetic exchange constants, the model predicts the spin-flip energies to be proportional to n.

We have also calculated two spin-flip values using LSDA+U and they show a markedly different behavior compared to the GGA. First, the LSDA+U spin flips are much larger than the GGA ones: 478 and 502 meV for $n=2$ and 3, respectively. Second, these values show an increase as a function of n at least for the two smallest clusters. Clearly, the on-site correction has a considerable effect on the short-ranged intracluster magnetic coupling. However, this difference is not crucial considering the Curie temperature, as will be discussed later.

B. Intercluster spin-flip energies

The relatively large intracluster spin-flip energies show that the Mn clusters form quite stable magnetic entities, and we expect that the long-ranged intercluster interactions will determine the nature of magnetism in the system at the macroscopic scale. To study the intercluster coupling, we calculate spin-flip energies ΔE of the entire clusters in hexagonal, monoclinic, and orthorhombic 48–108 atom supercells. In these cells, we set up clusters Mn_{n_1} and Mn_{n_2} ($n_1, n_2 = 1, \ldots, 4$) at varying distances and compare the total energies for parallel ($\uparrow_{n_1}+\uparrow_{n_2}$) and antiparallel ($\uparrow_{n_1}+\downarrow_{n_2}$) spin configurations to obtain ΔE. This is done without structural optimization, which is expected to have only a minor effect. As a test, we calculate ΔE for Mn_3-Mn_3 in a 108 atom supercell with and without structural optimization and obtain the very close values of 32 and 33 meV, respectively, justifying the omission of the optimization. The resulting ΔE's are presented in Fig. 5 as functions of r, the minimum distance between the cluster centers of mass. (Due to periodic images, there are more than one coupled cluster pair in each system.)

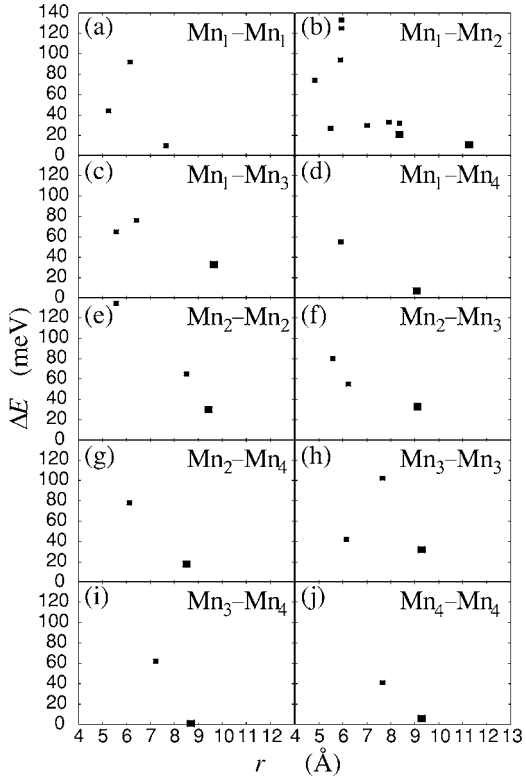

FIG. 5. Spin-flip energies ΔE for Mn_{n_1}-Mn_{n_2} cluster pairs as a function of separation of the cluster centers of mass, r. The small squares represent values obtained using supercells of 48 and 72 atoms, while the large squares are calculated in 96 and 108 atom cells. Some of the values are from Ref. 12.

We observe that the coupling is always ferromagnetic and spatially decaying, yet quite long ranged.[12,13] We also find that abnormally large spin-flip energies are obtained at the intercluster distances of $r \approx 6, \ldots, 8$ Å [Figs. 5(a), 5(b), 5(e), and 5(h)] which qualitatively agrees with Refs. 23, 38, and 39. Unlike in (Ga,Mn)As,[18] the strength of the coupling between clusters depends on the sizes of the clusters n_1 and n_2: Monomers couple relatively weakly to each other [Fig. 5(a)] and to tetramers [Fig. 5(d)] at long distances, while dimers

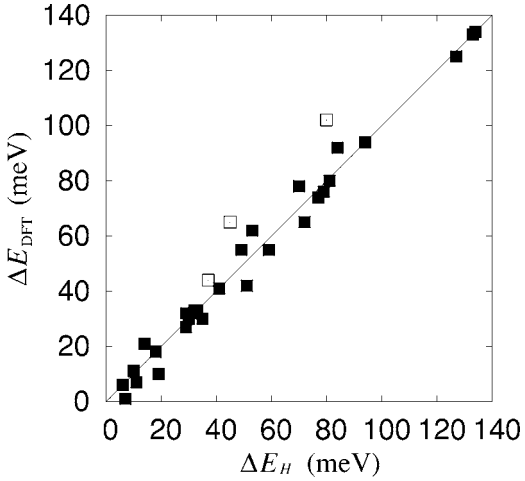

FIG. 6. The spin-flip energies ΔE given by DFT versus the same energies calculated from the effective Hamiltonian. The filled squares have been used in the fitting of the exchange function, while the open squares are additional points calculated in order to test consistency.

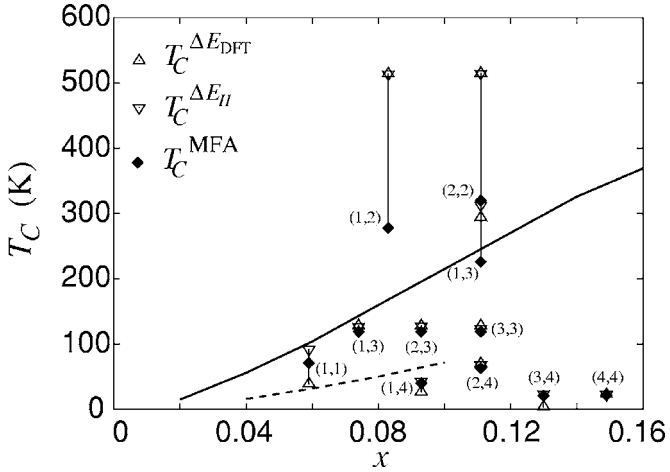

FIG. 7. Calculated Curie temperatures as a function of Mn concentration x. Solid and dashed lines represent T_C^{MC}'s for random and 1000 K clustered states, respectively (Ref. 13). T_C^{MFA} and $T_C^{\Delta E}$ values for ordered lattices are given as diamonds and triangles, respectively. $T_C^{\Delta E_{\mathrm{DFT}}}$ and $T_C^{\Delta E_H}$ are calculated from ΔE_{DFT} and ΔE_H, respectively. The cluster sizes in each lattice are given by the numbers in parentheses. Some of the $T_C^{\Delta E_{\mathrm{DFT}}}$ values are taken from Ref. 12.

[Figs. 5(b), 5(e), and 5(f)] and trimers [Figs. 5(c), 5(f), and 5(h)] interact more strongly even beyond several lattice constants. Tetramers altogether lose their ability to interact with other clusters beyond $r \gtrsim 9$ Å [Figs. 5(d), 5(g), 5(i), and 5(j)]. Changing from the GGA to LSDA+U has an effect on the intercluster spin-flip energies, but the change is not as dramatic as in the case of intracluster coupling.[12] We find the largest difference for a Mn_1-Mn_3 pair 6.13 Å apart, for which ΔE increases 50% from 76 to 117 meV when GGA is changed to LSDA+U. On average, LSDA+U yields higher spin-flip energies by some tens of percent but qualitatively the intercluster magnetic properties remain similar to those predicted by GGA.

The observed long-ranged magnetic coupling is different from coherent potential approximation (CPA) calculations,[39,40] where a short-ranged double-exchange mechanism is reported as the dominant interaction. While our results also show that a strong interaction exists at short distances, they also suggest the presence of an additional relatively long-ranged coupling mechanism. As the intercluster spin-flip energies are considerably smaller than the intracluster ones, the intercluster coupling will indeed be the dominating factor in determining the Curie temperature of the system at low Mn concentrations. Since the GGA and LSDA+U intercluster spin-flip energies are quite close to each other, the choice of functional should not have a dramatic effect on T_C^{MC}. Furthermore, since the LSDA+U energies for both intra- and intercluster spin flips are usually higher than the GGA ones, calculating the T_C^{MC} based on GGA values should avoid an overestimate.

Figure 6 shows the first-principles GGA spin-flip energies versus the corresponding energies calculated using the effective Hamiltonian [Eq. (1)] demonstrating quite a good agreement (see the Appendix for details on the mapping of the first-principles results onto the Hamiltonian). The figure also shows three open squares which were calculated afterward to verify the consistency of the fit. These DFT values deviate somewhat more from those predicted by the effective Hamiltonian; however, even in these cases the first-principles values are higher than the ones given by the effective Hamiltonian, which indicates that the fit does not overestimate the coupling strengths.

C. Curie temperatures

Curie temperatures calculated using the MC method (T_C^{MC}) and the MFA methods [T_C^{MFA} and $T_C^{\Delta E}$, Eq. (2)] are given in Fig. 7. The T_C^{MC} for a random system mimicking as-grown (Ga,Mn)N (solid line in Fig. 7) increases linearly as a function of x and reaches room temperature slightly below $x=0.14$ ($T_C^{\mathrm{MC}}=326$ K for $x=0.14$). We also find that clustering causes a dramatic drop in T_C^{MC} as seen by comparing the solid and dashed lines in Fig. 7 representing the random and clustered 1000 K equilibrium states, respectively. For example, at $x=0.10$, the random configuration value of 215 K is lowered to 72 K in a clustered state (for a more detailed discussion of the effects of clustering, see Ref. 13).

We also find that disorder decreases T_C^{MC}: When a regular Mn_1-Mn_2 lattice at $x \approx 0.08$ is changed to a random system with nearly the same Mn concentration, T_C^{MC} drops from 187 to 160 K. Similarly, changing from a regular Mn_1 lattice at $x=0.10$ to a random system causes the T_C^{MC} to drop from 246 to 215 K.[13] The result agrees qualitatively with Ref. 40 but our changes are smaller. The relatively small drops in T_C^{MC} we observe are due to the magnetic interactions extending quite far and having weak dependence on the intercluster distance r at the tail region $r \gtrsim 9$ Å [see, e.g., Fig. 5(b)]. The number of distant ($r \gtrsim 9$ Å) cluster pairs outweighs that of nearby ($r \lesssim 9$ Å) ones even though the latter interact more strongly. This makes T_C^{MC} relatively insensitive to the changes in r's that occur when changing from an ordered to a disordered configuration.

We next compare the Monte Carlo and mean-field methods for calculating Curie temperatures of ordered lattices. We obtain two sets of $T_C^{\Delta E}$ values by using both ΔE_{DFT} and ΔE_H in Eq. (2) (see Fig. 6). These values are shown in Fig. 7 as triangles for lattices where the clusters are set uniformly; i.e., the two clusters are set as far apart from each other as possible in the spanning supercell. The T_C^{MFA} values for the same lattices are shown in Fig. 7 as diamonds and the three mean-field values of a given system are connected with a vertical line. The highest $T_C^{\Delta E}$ values we obtain are approximately 514 K for the Mn_1-Mn_2 ($x=0.083$) and 515 K for the Mn_2-Mn_2 ($x=0.100$) supercells. These values are twice the corresponding T_C^{MC} ones (even for ordered lattices). The MFA neglecting internal degrees of freedom of the clusters as well as local fluctuations in magnetic ordering always overestimates the Curie temperature. However, since the spins in the studied systems exhibit long-ranged interactions, the mean-field treatment should be reasonable. In fact, Fig. 7 shows that most of the $T_C^{\Delta E}$ values obtained for the supercell systems are of the same order as the T_C^{MC} values—only the highest ΔE's lead to very high overestimates. This error is mostly due to the difference between T_C^{MFA} and $T_C^{\Delta E}$, as discussed in Sec. II. In the cases of the highest ΔE values, where the anomalously strong nearest-neighbor interactions occur (in the region $r \approx 6, \ldots, 8$ Å), our $T_C^{\Delta E}$ values are nearly twice the corresponding T_C^{MFA} ones. The T_C^{MFA} values, on the other hand, are not too bad overestimates since the ΔE approximation is not made. For instance, for the Mn_1-Mn_2 lattice with $x=0.083$, $T_C^{\Delta E}$ is about 514 K but calculating the sum of exchange coefficients using the fitted J's [Eq. (A8)] yields $\Sigma J=72$ meV and $T_C^{\mathrm{MFA}}=278$ K, i.e., 240 K lower than the value extracted straightforwardly from ΔE although still 90 K higher than the accurate Monte Carlo result $T_C^{\mathrm{MC}}=187$ K (for an identical ordered lattice). Although the T_C^{MFA} values, having been calculated for ordered lattices, appear as a rather scattered set of data points, further inspection reveals that they are actually in reasonable quantitative agreement with the T_C^{MC} values: The lattices with small clusters (the cluster sizes are given in parentheses in Fig. 7) have their T_C^{MFA} values close to the T_C^{MC} of the random state (solid line in Fig. 7) where also most of the Mn reside in monomers and dimers. The supercells with no more than four Mn ions in them even reasonably well capture a similar increasing trend as a function of x as seen in T_C^{MC}. Lattices with larger clusters have their T_C^{MFA} values closer to the T_C^{MC} of the clustered state (dashed line in Fig. 7), and especially the tetramer lattices show suppressed T_C^{MFA}'s. Thus, also the effect of clustering is clearly visible in the T_C^{MFA} results.

In a similar calculation for (Ga,As)Mn, we found T_C^{MC} to be slightly too high but otherwise a good quantitative estimate for the experimental Curie temperature.[41] Therefore, we expect that also in the case of (Ga,Mn)N the obtained values of T_C^{MC}, while possibly slightly overestimated, describe the Curie temperature semiquantitatively correctly.

V. CONCLUSIONS

We have studied the structures, formation energies, and magnetic interactions of various Mn clusters in (Ga,Mn)N by carrying out all-electron total-energy density-functional calculations. In agreement with previous results, we find that it is energetically favorable for the substitutional Mn ions to form clusters and that small clusters where the Mn ions surround one central N ion are especially stable. The energy gain associated with clustering has a maximum for tetramer formation, suggesting that the Mn clusters are most likely to be small. We find a relatively long-ranged magnetic interaction between the clusters and this coupling is strongest for dimers and trimers and weakest for tetramers. By mapping the density-functional spin-flip energies on an effective Hamiltonian, we calculate the Curie temperature T_C of the material using Monte Carlo methods. It is found that clustering has a strong, decreasing effect on T_C at all concentrations: for a random distribution of Mn ions, quite high T_C's are found while in a clustered state the Curie point is much lower. As a comparison, disorder has a much smaller effect compared to clustering due to the long-ranged interactions present. Curie temperatures calculated using the mean-field approximation (by evaluating the sum of exchange constants) are in reasonable agreement with the accurate Monte Carlo results. On the other hand, calculating T_C directly from energy differences between ferromagnetic and antiferromagnetic states can in some cases lead to high overestimates.[42]

ACKNOWLEDGMENTS

This work has been supported by the Academy of Finland through the Center of Excellence Program (2000–2011). H.R. and T.H. have been supported by the Finnish Cultural Foundation. The authors thank R. M. Nieminen, T. Ala-Nissilä, M. Alava, A. Harju, and A. Ayuela for many valuable discussions. The computing resources from the Center for Scientific Computing (CSC) are acknowledged.

APPENDIX: THE EFFECTIVE HAMILTONIAN

In this appendix, we derive the Hamiltonian used and present the assumptions made. We describe Mn spins by classical unit vectors $\mathbf{e}_{ik}$, where i is the cluster index and k is the index inside the cluster. The number of spins in cluster i is n_i. The Heisenberg Hamiltonian reads

$$\begin{aligned} H &= -\sum_{(ik,jk')} J_{ij}^{kk'} \mathbf{e}_{ik} \cdot \mathbf{e}_{jk'} \\ &= -\sum_{(i,j)} \sum_{k,k'} J_{ij}^{kk'} \mathbf{e}_{ik} \cdot \mathbf{e}_{jk'} - \sum_{i} \sum_{(k,k')} J_{ii}^{kk'} \mathbf{e}_{ik} \cdot \mathbf{e}_{ik'} \\ &= H_{\mathrm{inter}} + H_{\mathrm{intra}}, \end{aligned} \tag{A1}$$

where $(\cdot, \cdot)$ denotes a sum over pairs. The normalized spin of cluster i is given by the vector sum of the Mn ion spins

$$\mathbf{s}_i = \frac{1}{n_i} \sum_{k}^{n_i} \mathbf{e}_{ik}. \tag{A2}$$

The intercluster couplings in H_{inter} are approximated as

$$J_{ij}^{kk'} = J_{n_i n_j}(r_{ij}) n_i^{-1} n_j^{-1}, \tag{A3}$$

where r_{ij} is the distance between cluster centers i and j. $J_{n_i n_j}(r_{ij})$'s thus depend on intercluster distances and cluster

types but directional dependencies are excluded. Substituting expression (A3) in H_{inter} [Eq. (A1)] gives

$$H_{\text{inter}} = -\sum_{(i,j)} J_{n_i n_j}(r_{ij}) \left(\frac{1}{n_i} \sum_{k}^{n_i} \mathbf{e}_{ik} \right) \cdot \left(\frac{1}{n_j} \sum_{k'}^{n_j} \mathbf{e}_{jk'} \right) = -\sum_{(i,j)} J_{n_i n_j}(r_{ij}) \mathbf{s}_i \cdot \mathbf{s}_j. \quad \text{(A4)}$$

We do not use the Heisenbergian expression H_{intra} in Eq. (A1) for the intracluster interactions since it is incapable of describing the calculated total energies (see Sec. IV A). Instead, we describe the internal energies of clusters as functions of the effective spins,

$$H_{\text{intra}} = -\sum_{i} E_{n_i}(s_i). \quad \text{(A5)}$$

As our first-principles calculations are restricted to collinear spin configurations ($\uparrow_n$, $\uparrow_{n-1}\downarrow$, etc.), for which the effective spin s obtains values $S_n^m = (n-2m)/n$, $m=0,\ldots,n$, we set the values of $E_n(S_n^m)$ according to the calculated first-principles energies and interpolate for values of s in between. This is done so that for the dimer, we retain the usual $\mathbf{e}_1 \cdot \mathbf{e}_2$ coupling,

$$E_2(s) = E' - J\mathbf{e}_1 \cdot \mathbf{e}_2 = E_2(1) + [E_2(0) - E_2(1)](1 - s^2). \quad \text{(A6)}$$

The quadratic interpolation is generalized for other n straightforwardly by

$$s \in [S_n^{m+1}, S_n^m] \Rightarrow E_n(s) = E_n(S_n^m) + [E_n(S_n^{m+1}) - E_n(S_n^m)] \left[1 - \left(\frac{s - S_n^{m+1}}{S_n^m - S_n^{m+1}} \right)^2 \right]. \quad \text{(A7)}$$

This completes the construction of H_{intra} in Eq. (A1). The values $E_n(S_n^m)$ are given in Sec. IV A.

We determine the intercluster exchange coefficients $J_{n_i n_j}(r_{ij})$ by demanding that the spin-flip energies obtained using the effective Hamiltonian [Eqs. (A1)–(A7)] agree with the first-principles ones as closely as possible (in the least-squares sense). This is done by considering suitable functional forms for $J_{n_i n_j}(r)$ and fitting the energy values explicitly taking into account the periodicity of the calculated systems and the coupling to periodic images up to a cutoff distance, chosen as $r_{\text{cut}} = 13$ Å $\approx 4a$.

We examine first the Mn_1-Mn_2 pair, for which ten first-principles data points exist [see Fig. 5(b)]. Neglecting the anomalous ΔE values at $r \approx 6$ Å, we fit power-law and exponential functions to the spatially decaying part in $J_{12}(r)$. The best fit is obtained using a function $A_{12} r^{-3}$ with $A_{12} = 3.00$ eV Å^3. In order to represent the anomalous ΔE values neglected thus far, we add a local correction term $B_{12}(r - r_{12}^a)\exp[-\alpha_{12}(r - r_{12}^b)^2]$, which yields the best fit with parameters $B_{12} = 302$ meV Å^{-1}, $r_{12}^a = 5.59$ Å, $r_{12}^b = 5.69$ Å, and $\alpha_{12} = 16.3$ Å^{-2}. The difference between spin-flip energies (per cluster pair) given by DFT and the effective Hamiltonian remains less than 7 meV in all cases and the relatively good fit also suggests that using the Heisenberg-type model for the intercluster couplings is justified. The coupling function is generalized for other cluster pairs by assuming the same functional form

$$J_{n_i n_j}(r) = \frac{A_{n_i n_j}}{r^3} + B_{n_i n_j}(r - r_{n_i n_j}^a) e^{-\alpha_{n_i n_j}(r - r_{n_i n_j}^b)^2}. \quad \text{(A8)}$$

However, due to computational reasons, we have been able to calculate only few data points for each cluster pair (Fig. 5), and so we further assume that the shape of the local correction and its height with respect to the decaying part are the same in all cases; i.e., that $r_{n_i n_j}^b - r_{n_i n_j}^a$, $\alpha_{n_i n_j}$, and $B_{n_i n_j}/A_{n_i n_j}(r_{n_i n_j}^a)^{-3}$ are constants. This leaves only $A_{n_i n_j}$ and $r_{n_i n_j}^a$ as free parameters, which are then fitted to the first-principles data. The obtained parameter values are given in Table I (see also Ref. 13). The highest $A_{n_i n_j}$ are obtained for dimers and trimers and the lowest for tetramers. Note that if the intercluster coupling was described as a sum of separate Mn-Mn couplings, we would expect $A_{n_i n_j} \propto n_i n_j$ [cf. Eq. (A3)], which is clearly not the case. Therefore, it is important that the coupling is studied separately for all cluster pairs. It should also be noted that although directional dependencies in the exchange coupling may in some cases be important,[43,44] consistency between our model and the DFT results is good even though directional effects have been neglected (see Fig. 6).

To complete the construction of the effective Hamiltonian, we must properly define the clusters into which the Mn ions are grouped. Our cluster locating algorithm works as follows: (i) Mark all Mn ions in the system as being "free" and set $n=4$. (ii) Scan the system. If a N ion with n free Mn nearest neighbors is found, mark them as one Mn_n cluster

TABLE I. Parameters $A_{n_i n_j}$ (given in multiples of $A_{11} = 1.5$ eV Å^{-3}) and $r_{n_i n_j}^a$ (in Å) for the fitted exchange functions [Eq. (A8)].

(n_i, n_j)	$A_{n_i n_j}$	$r_{n_i n_j}^a$	(n_i, n_j)	$A_{n_i n_j}$	$r_{n_i n_j}^a$
(1,1)	1.0	5.9	(2,3)	2.8	6.3
(1,2)	2.0	5.6	(2,4)	1.5	5.9
(1,3)	2.8	5.8	(3,3)	2.8	6.5
(1,4)	0.9	5.7	(3,4)	0.8	7.0
(2,2)	2.8	5.4	(4,4)	0.5	7.3

("nonfree"). (iii) Once completed, set $n=n-1$. Finish if $n=0$, otherwise return to step (ii). Summarizing, we define a cluster as a collection of Mn ions with a common nearest-neighbor N with the restriction that each Mn ion can belong to only one cluster. In this way, for instance, a ring-shaped trimer is treated as a dimer and a monomer and a planar tetramer as a trimer and a monomer. This is not a unique grouping, but the ionic relaxations and the result that the N-centered clusters are the most stable structures support this definition. The definition also fixes the maximum cluster size to Mn_4, and therefore we know the functions $J_{n_i n_j}(r)$ for all cluster pairs. Although the exchange interactions for dimers and trimers have been studied using only the *a*-plane configurations of Mn_2 and Mn_3, we assume that tilted configurations behave similarly. When generating simulation geometries, we randomly deposit clusters in the lattice according to a predetermined size distribution. Once the generation is completed, the cluster distribution is recalculated to check that the grouping is correct. If the distribution is not correct (e.g., two dimers are set next to each other and form a trimer and a monomer), clusters are removed and added as needed until the required distribution is reached.

*Corresponding author. Electronic address: tjh@fyslab.hut.fi
†Present address: National Renewable Energy Laboratory, Golden, CO 80401, USA.

[1] H. Munekata, H. Ohno, S. von Molnar, A. Segmüller, L. L. Chang, and L. Esaki, Phys. Rev. Lett. **63**, 1849 (1989).
[2] H. Ohno, Science **281**, 951 (1998).
[3] T. Dietl, H. Ohno, F. Matsukura, J. Cibert, and D. Ferrand, Science **287**, 1019 (2000).
[4] M. L. Reed, N. A. El-Masry, H. H. Stadelmaier, M. K. Ritums, M. J. Reed, C. A. Parker, J. C. Roberts, and S. M. Bedair, Appl. Phys. Lett. **79**, 3473 (2001).
[5] M. E. Overberg, C. R. Abernathy, S. J. Pearton, N. A. Theodoropoulou, K. T. McCarthy, and A. F. Hebard, Appl. Phys. Lett. **79**, 1312 (2001).
[6] T. Sasaki, S. Sonoda, Y. Yamamoto, K. Suga, S. Shimizu, K. Kindo, and H. Hori, J. Appl. Phys. **91**, 7911 (2002).
[7] G. T. Thaler, M. E. Overberg, B. Gila, F. Frazier, C. R. Abernathy, S. J. Pearton, J. S. Lee, S. Y. Lee, Y. D. Park, Z. G. Khim, J. Kim, and F. Ren, Appl. Phys. Lett. **80**, 3964 (2002).
[8] S. Dhar, O. Brandt, A. Trampert, L. Däweritz, K. J. Friedland, K. H. Ploog, J. Keller, B. Beschoten, and G. Güntherodt, Appl. Phys. Lett. **82**, 2077 (2003).
[9] M. Sato, H. Tanida, K. Kato, T. Sasaki, Y. Yamamoto, S. Sonoda, S. Shimizu, and H. Hori, Jpn. J. Appl. Phys., Part 1 **41**, 4513 (2002).
[10] B. K. Rao and P. Jena, Phys. Rev. Lett. **89**, 185504 (2002).
[11] G. Bouzerar, T. Ziman, and J. Kudrnovský, Appl. Phys. Lett. **85**, 4941 (2004).
[12] T. Hynninen, H. Raebiger, A. Ayuela, and J. von Boehm, Appl. Phys. Lett. **88**, 122501 (2006).
[13] T. Hynninen, H. Raebiger, and J. von Boehm, J. Phys.: Condens. Matter **18**, 1561 (2006).
[14] M. van Schilfgaarde and O. N. Mryasov, Phys. Rev. B **63**, 233205 (2001).
[15] L. M. Sandratskii, P. Bruno, and S. Mirbt, Phys. Rev. B **71**, 045210 (2005).
[16] L. M. Sandratskii and P. Bruno, J. Phys.: Condens. Matter **16**, L523 (2004).
[17] H. Raebiger, A. Ayuela, and R. M. Nieminen, J. Phys.: Condens. Matter **16**, L457 (2004).
[18] H. Raebiger, A. Ayuela, and J. von Boehm, Phys. Rev. B **72**, 014465 (2005).
[19] J. L. Xu, M. van Schilfgaarde, and G. D. Samolyuk, Phys. Rev. Lett. **94**, 097201 (2005).
[20] G. Kresse and J. Furthmüller, Phys. Rev. B **54**, 11169 (1996); *VASP: The Guide* (Vienna University of Technology, Vienna, 1999), http://cms.mpi.univie.ac.at/vasp/vasp/vasp.html
[21] S. L. Dudarev, G. A. Botton, S. Y. Savrasov, C. J. Humphreys, and A. P. Sutton, Phys. Rev. B **57**, 1505 (1998).
[22] L. M. Sandratskii, P. Bruno, and J. Kudrnovský, Phys. Rev. B **69**, 195203 (2004).
[23] M. Wierzbowska, D. Sánchez-Portal, and S. Sanvito, Phys. Rev. B **70**, 235209 (2004).
[24] H. Monkhorst and J. Pack, Phys. Rev. B **13**, 5188 (1976).
[25] A. Eichler, J. Hafner, J. Furthmüller, and G. Kresse, Surf. Sci. **346**, 300 (1996).
[26] C. Domb and M. F. Sykes, Phys. Rev. **128**, 168 (1962).
[27] U. Wolff, Phys. Rev. Lett. **62**, 361 (1989).
[28] N. Metropolis, A. W. Rosenbluth, M. N. Rosenbluth, A. H. Teller, and E. Teller, J. Chem. Phys. **21**, 1087 (1953).
[29] K. Binder, Phys. Rev. Lett. **47**, 693 (1981).
[30] K. Sato, P. H. Dederichs, and H. Katayama-Yoshida, Europhys. Lett. **61**, 403 (2003).
[31] Ph. Kurz, G. Bihlmayer, and S. Blügel, J. Phys.: Condens. Matter **14**, 6353 (2002).
[32] I. Turek, J. Kudrnovský, G. Bihlmayer, and S. Blügel, J. Phys.: Condens. Matter **17**, 2771 (2003).
[33] S. J. Pearton, C. R. Abernathy, M. E. Overberg, G. T. Thaler, D. P. Norton, N. Theodoropoulou, A. F. Hebard, Y. D. Park, F. Ren, J. Kim, and L. A. Boatner, J. Appl. Phys. **93**, 1 (2003).
[34] M. Marques, L. K. Teles, L. M. R. Scolfaro, J. Furthmüller, F. Bechstedt, and L. G. Ferreira, Appl. Phys. Lett. **86**, 164105 (2005).
[35] R. Basewicz, J. Filipowicz, S. Podsiado, T. Szyszko, and M. Kamiński, J. Phys. Chem. Solids **64**, 1469 (2003).
[36] Y. L. Soo, G. Kioseoglou, S. Kim, S. Huang, Y. H. Kao, S. Kuwabara, S. Owa, T. Kondo, and H. Munekata, Appl. Phys. Lett. **79**, 3926 (2001).
[37] Q. Wang, Q. Sun, P. Jena, and Y. Kawazoe, Phys. Rev. Lett. **93**, 155501 (2004).
[38] B. Sanyal, O. Bengone, and S. Mirbt, Phys. Rev. B **68**, 205210 (2003).
[39] K. Sato, W. Schweika, P. H. Dederichs, and H. Katayama-Yoshida, Phys. Rev. B **70**, 201202(R) (2004).
[40] L. Bergqvist, O. Eriksson, J. Kudrnovský, V. Drchal, P. Korzhavyi, and I. Turek, Phys. Rev. Lett. **93**, 137202 (2004).
[41] T. Hynninen, M. Ganchenkova, H. Raebiger, and J. von Boehm, Phys. Rev. B **74**, 195337 (2006).

[42] Y. D. Park, A. T. Hanbicki, S. C. Erwin, C. S. Hellberg, J. M. Sullivan, J. E. Mattson, T. F. Ambrose, A. Wilson, G. Spanos, and B. T. Jonker, Science **295**, 651 (2002).
[43] J. Kudrnovský, I. Turek, V. Drchal, F. Máca, P. Weinberger, and P. Bruno, Phys. Rev. B **69**, 115208 (2004).
[44] P. Mahadevan, A. Zunger, and D. D. Sarma, Phys. Rev. Lett. **93**, 177201 (2004).